Fugitive Inks for Direct-Write Assembly of Three-Dimensional Microvascular Networks**

By *Daniel Therriault*, *Robert F. Shepherd*, *Scott R. White*,* and *Jennifer A. Lewis**

Microfluidic systems are essential to a broad range of technological applications, including biotechnology,[1] microelectronics,[2] sensors,[3] chemical reactors,[4] and autonomic materials.[5] Several approaches have emerged for fabricating two-dimensional (2D)[6] and three-dimensional (3D)[7] microfluidic devices, including photolithographic or soft-lithographic techniques,[1b,2a,3c,4b,5b] laser micromachining,[7b] and derivative methods based on soft lithography.[7d–f] These techniques, however, have been confined to relatively thin device architectures (of only a few layers) and limited by materials constraints,[7b] poor resolution,[7c] or the need for extensive manual labor.[7d–f] We recently demonstrated the direct-write assembly of 3D microvascular networks, consisting of 16-layer structures with interconnected microchannels (200 μm in diameter) encapsulated in an epoxy matrix.[7a] Our approach involved the robotic deposition of a fugitive organic ink, which yields the desired microchannel network upon its subsequent removal from the matrix. Difficulties such as deformation of this fugitive-ink scaffold were encountered during assembly that prevented fabrication of larger 3D structures. Here, we report the development of a new fugitive ink that enables the direct-write assembly of 3D scaffolds (with more than a hundred layers) that retain their shape during fabrication and subsequent matrix infiltration under ambient conditions.

The fabrication procedure of 3D microvascular networks (see Scheme 1) begins with the robotic deposition[8] of the fugitive ink onto a moving *x*–*y* platform, yielding a 2D pattern. After the initial layer is generated, the deposition nozzle, which is mounted on the *z*-stage, is raised a finite height and another layer is deposited. This process is repeated until the desired 3D scaffold is created. The interstitial pore space between patterned features is then infiltrated with a low-viscosity epoxy. Upon curing, the ink-based scaffold is removed, yielding an interconnected 3D microvascular network. The fugitive inks used in this directed assembly technique must satisfy several criteria. First, the ink must flow through a fine

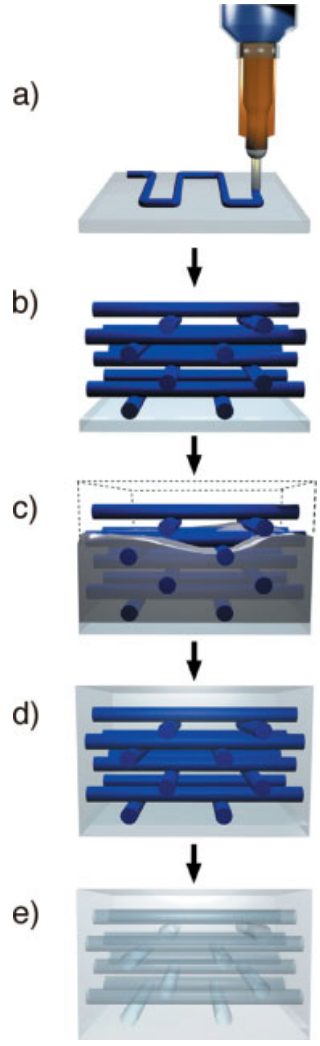

Scheme 1. Schematic representation of the fabrication procedure for 3D microvascular networks by direct-write assembly: a) deposition of fugitive ink (in blue) through cylindrical nozzle; b) multilayer scaffold after ink deposition; c) resin infiltration into scaffold; d) resin solidification to form structural matrix; and e) 3D microvascular network created after removal of fugitive ink.

[*] Prof. J. A. Lewis, R. F. Shepherd
Frederick Seitz Materials Research Laboratory
Materials Science and Engineering Department
NSF Center for Directed Assembly of Nanostructures
University of Illinois at Urbana-Champaign
212d Ceramics Bldg., 1304 W. Green St.
Urbana, IL 61801 (USA)
E-mail: jalewis@staff.uiuc.edu

Prof. S. R. White
Advanced Chemical Systems Group
Beckman Institute for Advanced Science and Technology
Aerospace Engineering Department
University of Illinois at Urbana-Champaign
306 Talbot Lab, 104 S. Wright St.
Urbana, IL 61801 (USA)
E-mail: swhite@uiuc.edu

Prof. D. Therriault
Mechanical Engineering Department
École Polytechnique de Montréal
Montréal, Québec H3C 3A7 (Canada)

[**] The authors gratefully acknowledge funding for this project provided by AFOSR Aerospace and Materials Science Directorate (Grant # F49620-03-1-0179), U.S. Department of Energy, Division of Materials Science under Award No. DEFG02-91ER45439 through the Frederick Seitz Materials Research Laboratory (UIUC), and the NSF Center for Directed Assembly of Nanostructures (Grant No. DMR-01-177792). The robotic deposition apparatus used in this work was designed and built by J. Cesarano, and the customized software for the 3D fabrication was developed by J. E. Smay. Partial support for D. Therriault was provided by the University of Illinois Nanoscience and Technology Center Fellowship and the government of Québec (NATEQ).

DOI: 10.1002/adma.200400481

ADVANCED MATERIALS

deposition nozzle under high shear, yet be self-supporting even as it spans gaps in the underlying layer(s). Second, the ink-based scaffold must maintain its shape during resin infiltration. Finally, the ink scaffold must liquefy at a moderate temperature (~60 °C) to facilitate its removal from the templated matrix. The fugitive ink used in our original work[7a] consisted of a mixture of paraffin wax, mineral oil, and ferric ferrocyanide nanoparticles (~2.2 wt.-%), and was not suitable for writing under ambient conditions. To meet these criteria, temperatures of ~19 °C and –70 °C were required for ink deposition and scaffold infiltration, respectively.[7a] While one could alter the ink rheology by increasing the nanoparticle-filler concentration, these species were difficult to fully remove from the microchannels during the liquefaction and subsequent cleaning procedures. Moreover, direct-write assembly of 3D scaffolds using these nanoparticle-filled inks were limited to low-aspect-ratio spanning filaments (i.e., $L/d < 6$, where L is the unsupported distance and d is the filament diameter) to minimize scaffold deformation.

To overcome these challenges, we have developed a new fugitive ink comprised of a binary mixture of microcrystalline wax (weight-average molecular weight $M_w = 1450\ g\,mol^{-1}$) and a lower M_w organic phase. Its mechanical properties were tailored by varying the relative amounts of each constituent in the absence of nanoparticle fillers. The ink rheology was investigated as a function of composition using a controlled-stress rheometer. The ink elasticity, as characterized by the plateau value of the storage shear modulus (G'), increased linearly from ~0.1 MPa to 1 MPa with increasing weight fraction of microcrystalline wax under ambient conditions (Fig. 1a). The ink performance was further evaluated by depositing 3D scaffold networks under ambient conditions. Inks rich in microcrystalline wax (>50 wt.-%) were difficult to extrude through the deposition nozzle at applied pressures below 3 MPa (nozzle diameter of 200 μm) and the resulting extruded filament frequently ruptured, whereas inks with lower wax contents (10–40 wt.-%) exhibited excellent printing behavior under these conditions. The optimal ink composition for direct writing was determined to be 40 wt.-% microcrystalline wax, since it exhibited the highest G' value while still maintaining excellent deposition capability at modest applied pressure. In this case, the finest ink filament that could be continuously extruded was ~10 μm in diameter. Figure 1b shows a plot of ink elasticity as a function of shear stress for the binary organic ink (40 wt.-% microcrystalline wax). As a benchmark, the data obtained for the original (nanoparticle-filled) fugitive ink is also included. Both the shear yield stress (τ_y) and G' values observed for the optimized binary organic ink exceed the values reported for the nanoparticle-filled organic ink by more than an order of magnitude under ambient conditions. Hence, this new ink features the proper compromise between superior stiffness (e.g., G') for self-supporting behavior and a moderate shear yield stress for facile extrusion through the deposition nozzle.

The time-dependent relaxation (or deformation) behavior of each fugitive ink was studied by optically imaging free-standing ink filaments produced by robotic deposition. Representative optical images of ink filaments spanning 10 mm gaps are shown in Figures 2a,b for the original organic and binary fugitive inks, respectively. As evident in Figure 2b, the binary organic ink filament experiences significantly less deformation over the timescale of the experiment relative to filaments produced from the original fugitive ink. The mid-span deflections as a function of time for both inks were quantified by image analysis, as shown in Figure 2c. Both inks displayed similar deformation behavior, with an initially high deflection rate followed by gradual retardation before reaching a constant, lower deflection rate. However, the binary organic-ink

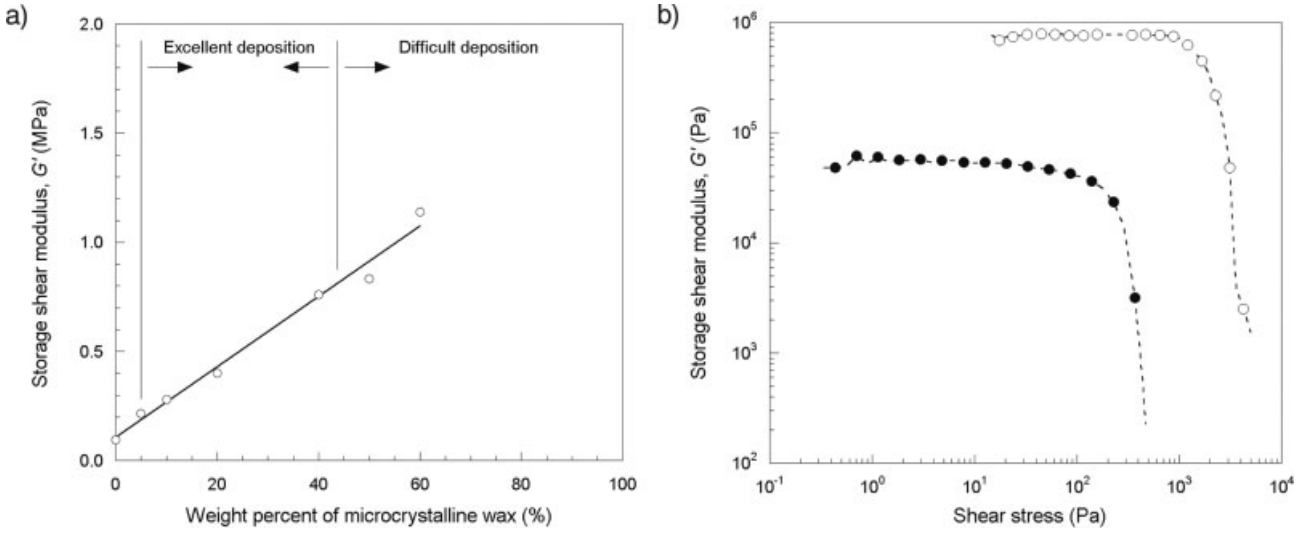

Figure 1. a) Low shear, plateau storage modulus of binary organic inks as a function of microcrystalline wax content (where the solid line is a linear curve fit $y = mx + b$, with $m = 16.16\ kPa\,\%^{-1}$ and $b = 105$ kPa); $T = 25$ °C. b) Storage shear modulus as a function of applied stress for nanoparticle-filled organic ink (●) and binary organic ink (○, 40 wt.-% microcrystalline wax.)

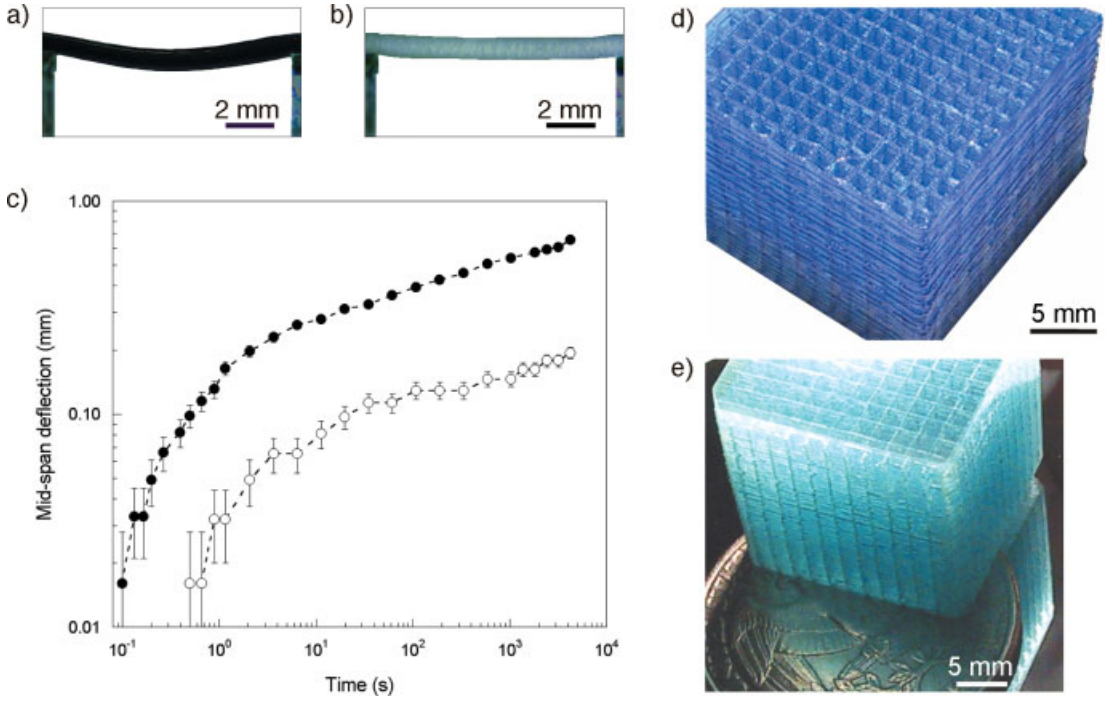

Figure 2. Optical images (side view) of spanning filament ($L = 10$ mm and $L/d \sim 9.3$) held for ~1 h at $T = 20\,^{\circ}C$ of a) particle-filled organic ink and b) binary organic ink. c) Plot of mid-span deflection as a function of time for nanoparticle-filled organic ink (●) and binary organic ink (○). d) Optical image of a 104-layer scaffold assembled from the binary organic ink (40 wt.-% microcrystalline wax) deposited through a 200 μm nozzle. (Note: Blue pigment particles were added to the binary organic ink for easier visualization.) e) Optical image of a 104-layer microvascular network enclosed in clear epoxy matrix, with a quarter-dollar coin for scale.

filament only exhibited 0.18 mm mid-span deflection after 1 h at 20 °C, whereas the nanoparticle-filled organic ink developed a significantly larger deflection of 0.63 mm. The initial period ($t < 10$ s) of rapid relaxation stems from the viscoelastic recovery that occurs immediately after the ink exits the deposition nozzle. Within the nozzle, the ink yields under high shear ($\tau > \tau_y$). Thus, immediately upon exiting the nozzle ($\tau \sim 0$), its elastic response is quite low. Ultimately, the ink recovers to its plateau G' value, as revealed by the onset of a reduced deflection rate at $t \geq 10$ s.

The binary organic ink enables the direct-write assembly of 3D scaffolds with higher aspect ratios and improved shape retention under ambient conditions. As an example, we created a 3D scaffold consisting of a 104-layer structure of parallel cylindrical rods with an inter-rod separation distance of 1.25 mm ($L/d = 6.25$), as shown in Figure 2d. This structure was produced by robotically depositing a binary organic ink (40 wt.-% microcrystalline wax) at a deposition speed of 8 mm s^{-1} and with an extrusion pressure of 2.9 MPa. This 3D ink scaffold structure retained its shape during immersion into a reservoir of uncured epoxy resin and subsequent curing under ambient conditions. After solidification, the fugitive-ink scaffold was removed by heating to ~75 °C under a light vacuum, leaving behind the interconnected microchannel array shown in Figure 2e. The resulting 3D microvascular network consists of 1664 microchannels embedded in a 20 mm × 20 mm × 20 mm cube with a total pore volume of ~13 %. Note that the individual channels within the network were straight and well connected with minimal irregularities (e.g., a slight waviness), as observed by fluorescence microscopy of the dye-filled channels.

Highly efficient fluid-mixing devices can be created within these 3D microvascular networks using standard photolithographic techniques.[7a] Complex 3D mixing elements, such as square-spiral towers, have been previously demonstrated in earlier microvascular networks.[7a] To explore other mixing-tower architectures, we created a 32-layer triangular scaffold of ink filaments ($d = 200$ μm) with an inter-rod separation of 1.60 mm from the binary organic ink (Fig. 3a). Upon subsequent matrix infiltration, curing, and ink removal, we produced a 3D microvascular network of interconnected microchannels embedded in an epoxy matrix (Fig. 3b). Triangular-spiral mixing towers were then introduced within this 3D network by first infiltrating the microchannels with a photocurable resin, followed by subsequent patterning and UV irradiation. After the photopolymerization, the unreacted resin was drained under a light vacuum, leaving behind the desired patterned network. The fluorescence microscopy image in Figure 3c shows a cross-sectional view of adjacent triangular towers coupled by microchannel conduits, while Figure 3d shows a top view of an isolated triangular tower. Significant enhancements in fluid mixing were observed for these triangular mixing elements (data not shown); however, the observed enhancement was analogous to that reported previously for the square-spiral towers.[7a]

ADVANCED MATERIALS

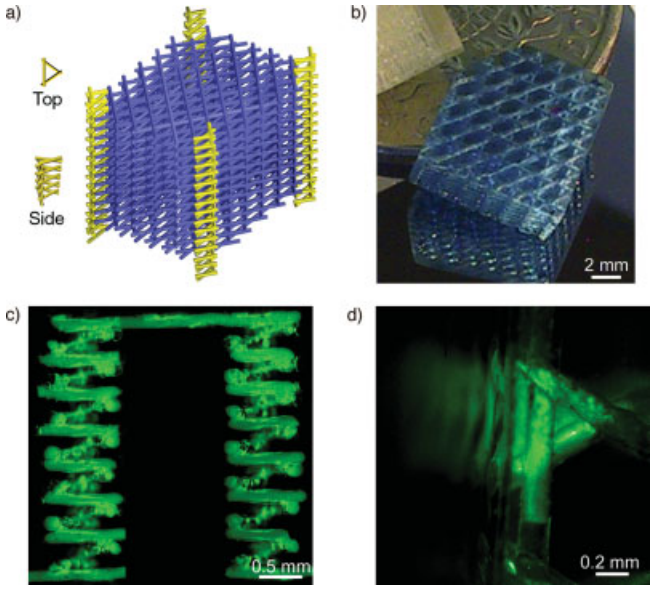

Figure 3. Patterning of triangular-spiral towers: a) Schematic representation of triangular tower structure (yellow) embedded within the 3D microvascular network (blue). b) Optical image of epoxy matrix with 3D microvascular network of 32 layers (triangular pattern) placed beside a quarter-dollar coin. Fluorescence microscope images of the c) side and d) top views of a fluid-filled triangular tower embedded inside an epoxy matrix.

By developing new fugitive inks based on a binary mixture of organic species, we have greatly extended our capability to create 3D microvascular networks via direct-write assembly. These new inks enable the ambient deposition of 3D scaffolds with unparalleled high aspect ratios and device complexities. Such advances open up new opportunities for microfluidic systems for a broad range of technological applications including chaotic mixers,[7a] autonomic healing materials,[5a] and self-cooling polymer structures.[2a]

Experimental

Binary organic inks were prepared by first melting (at ~80 °C) a low weight-average molecular weight (M_w) organic constituent ($M_w = 840$ g mol^{-1}, Vaseline petroleum jelly, Chesebrough-Pond's, Ladson, SC) and then adding an appropriate amount of microcrystalline wax ($M_w = 1450$ g mol^{-1}, SP 18, Strahl & Pitsch, Inc., West Babylon, NY). These constituents were mixed together by magnetic stirring for 20 min. The M_w of each constituent was determined by gel permeation chromatography (TDA Model 300, Viscotek, Houston, TX) using tetrahydrofuran.

The nanoparticle-filled organic ink (Prussian blue paste, Loctite, Rocky Hill, CT) used previously [7a] is commercially available and serves as a benchmark in the current study. It consists of a mixture of paraffinic hydrocarbon wax, mineral oil, and ferric ferrocyanide nanoparticles ($Fe_4[Fe(CN)_6]_3$) with typical sizes of 20–150 nm [9].

The complex shear modulus ($G^* = G' + iG''$, where G' is the storage shear modulus and G'' is the loss shear modulus) and yield stress (τ_y) were measured using a controlled-stress rheometer (Bohlin CVOR-200 apparatus, Cranbury, NJ) fitted with a concentric-cylinder geometry C-14 cell. An appropriate amount (3 mL) of the ink was melted at ~75 °C and poured into the cell, which was cooled to the desired temperature using a controlled-temperature circulating bath (Model 9110, Polyscience, Chicago, IL). Oscillatory-shear experiments were then carried out at 1 Hz in which the stress amplitude was incrementally increased.

The time-dependent deflection of an ink filament spanning a rigid support structure was measured at 20 °C. Prior to the experiment, a thermal equilibrium period of ~15 min ensured a uniform ink temperature within the deposition nozzle (syringe with barrel diameter = 4.6 mm, EFD Inc., East Providence, RI) and the support structure, both controlled by a F25-EC circulator (Julabo, Allentown, PA). A 1.07 mm filament was deposited using a robotic deposition apparatus (Model JL2000, Robocasting Enterprises, Inc., Albuquerque, NM) over a 10 mm spanning distance (distance L and filament diameter d so that $L/d \sim 9.3$). Filaments were deposited from both the binary and nanoparticle-filled organic inks at a deposition speed of 6 mm s^{-1} and extrusion pressures of 358 kPa and 103 kPa, respectively. After deposition, the filaments were imaged with a video camera through a microscope lens (magnification 5×, Edmund Optics, Barrington, NJ) from a side-view perspective for a period of 1 h. A thermocouple was inserted inside the ink filament (at the supported section) to directly monitor the ink temperature. The deflection history was obtained from a series of digital images that were stored on the computer using a video analog–digital converter (Moviestar Version 5, Dazzle, Mountain View, CA). The video signal operated at 30 frames s^{-1} ($\Delta t = 0.033$ s) with a resolution of 720 pixels × 480 pixels (1 pixel ~ 0.014 mm at 5× magnification). Image processing was carried out using Photoshop (Version 6, Adobe, San Jose, CA), from which the mid-span deflection of each filament was determined as a function of time at ~30 time intervals equally spaced on a logarithmic scale ranging from 0.033 s to 4258 s. The initial data point ($t = 0.033$ s) was recorded when the filament first contacted the second rigid support upon exiting the nozzle.

Three-dimensional (3D) microvascular scaffolds were fabricated using the robotic deposition apparatus. The three-axis motion of the x–y and z-stages was independently controlled by a custom-designed computer program (Robocad Version 2.0) that allowed for the construction of 3D structures in a layer-by-layer build sequence. The binary organic ink was housed in a syringe (barrel diameter = 4.6 mm, EFD Inc.) and deposited through a nozzle (diameter = 200 μm) onto a porous Teflon substrate (Airtech Performance Products, Huntington Beach, CA) at room temperature. An air-powered dispensing system (HP7X, EFD Inc.) provided an extrusion pressure of 2.9 MPa for deposition at a constant x–y table speed of 8 mm s^{-1}. The 104-layer scaffold consisted of a simple cubic lattice of 20 mm × 20 mm × 20 mm with an inter-rod spacing of 1.25 mm. The initial layer of the 3D triangular structure was composed of a parallel array of rods with an inter-rod spacing of 1.60 mm. The two subsequent layers were printed by rotating each layer by 60° combined with a planar shift of 0.8 mm with respect to the underlying layer. This three-layer sequence was repeated until the desired 3D scaffold was patterned (32 layers, ~6 mm high). To promote intimate contact between layers, a layer spacing Δz of $0.90d$ was used in the fabrication process. The total deposition time for the 104-layer and 32-layer scaffolds was ~1.3 h and ~15 min, respectively. Each scaffold was then slowly immersed into a bath of the uncured resin (Epoxy 20-332, Epoxy Etc., Cranston, RI) under ambient conditions. The resin was cured at 22 °C for 24 h and then at 60 °C for 2 h. At 75 °C, the scaffold liquefied and was removed under a light vacuum, yielding the desired microvascular network of interconnected cylindrical microchannels. A vacuum pump (Duoseal, Welch Scientific, Buffalo Grove, IL) linked to a vacuum trap was used to remove the melted organic ink through a small tube attached to the opened microchannels.

Subsequent patterning of triangular spiral towers was carried out by infiltrating a photopolymerizable resin (Model 61, Norland Products, Cranebury, NJ) into the microchannels of the 3D microvascular network. This structure was then masked, and selected microchannels were polymerized by UV flood exposure for 60 s. The photomask was generated by printing the desired pattern on a transparency using a high-resolution printer (5080 dots per inch). A filtered 100 W UV lamp (U-MNUA, type BP360-370, 360 nm wavelength) was mounted on an Olympus (Melville, NY) epi-fluorescence microscope (BX-60) with a 2× objective.

Optical images of the 3D microvascular network were captured by a Canon 141 Digital Camera (Canon U.S.A, Inc., Lake Success, NY). Fluorescence microscope images were obtained with a Zeiss Axiovert 100 fluorescence light microscope (Carl Zeiss Microimaging, Thornwood, NY) with a 2.5 × objective.

Received: March 29, 2004
Final version: October 15, 2004

[1] a) A. Strömberg, A. Karisson, F. Ryttsén, M. Davidson, D. T. Chiu, O. Orwar, *Anal. Chem.* **2001**, *73*, 126. b) H.-P. Chou, C. Spence, A. Scherer, S. Quake, *Proc. Natl. Acad. Sci. U. S. A.* **1999**, *96*, 11.

[2] a) G. J. Snyder, J. R. Lim, C.-K. Huang, J.-P. Fleurial, *Nat. Mater.* **2003**, *2*, 528. b) Y. Mizukami, D. Rajniak, A. Rajniak, M. Nishimura, *Sens. Actuators, B* **2002**, *81*, 2002.

[3] a) M. L. Chabinyc, D. T. Chiu, J. C. McDonald, A. D. Stroock, J. F. Christian, A. M. Karger, G. M. Whitesides, *Anal. Chem.* **2001**, *73*, 4491. b) A. E. Kamholz, B. H. Weigl, B. A. Finlayson, P. Yager, *Anal. Chem.* **1999**, *71*, 5340. c) J.-C. Roulet, R. Völkel, H. P. Herzig, E. Verpoorte, N. F. de Rooij, R. Dändliker, *J. Microelectromech. Syst.* **2001**, *10*, 1057.

[4] a) M. W. Losey, M. A. Schmidt, K. F. Jensen, *Ind. Eng. Chem. Res.* **2001**, *40*, 2555. b) S. K. W. Dertinger, D. T. Chiu, N. L. Jeon, G. M. Whitesides, *Anal. Chem.* **2001**, *73*, 1240.

[5] a) S. R. White, N. R. Sottos, P. H. Geubelle, J. S. Moore, M. R. Kessler, S. R. Sriram, E. N. Brown, S. Viswanathan, *Nature* **2001**, *409*, 794. b) D. J. Beebe, J. S. Moore, J. M. Bauer, Q. Yu, R. H. Liu, C. Devadoss, B.-H. Jo, *Nature* **2000**, *404*, 588.

[6] a) D. J. Beebe, J. S. Moore, Q. Yu, R. H. Liu, M. L. Kraft, B.-H. Jo, C. Devadoss, *Proc. Natl. Acad. Sci. U. S. A.* **2000**, *97*, 13 488. b) J. C. McDonald, D. C. Duffy, J. R. Anderson, D. T. Chiu, H. Wu, O. J. A. Schueller, G. M. Whitesides, *Electrophoresis* **2000**, *21*, 27.

[7] a) D. Therriault, S. R. White, J. A. Lewis, *Nat. Mater.* **2003**, *2*, 265. b) S. J. Qin, W. J. Li, *Sens. Actuators, A* **2002**, *97–98*, 749. c) J. C. McDonald, M. L. Chabinyc, S. J. Metallo, J. R. Anderson, A. D. Stroock, G. M. Whitesides, *Anal. Chem.* **2002**, *74*, 1537. d) H. Wu, T. W. Odom, D. T. Chiu, G. M. Whitesides, *J. Am. Chem. Soc.* **2003**, *125*, 554. e) J. R. Anderson, D. T. Chiu, R. J. Jackman, O. Cherniavskaya, J. C. McDonald, H. Wu, S. H. Whitesides, G. M. Whitesides, *Anal. Chem.* **2000**, *72*, 3158. f) B.-H. Jo, L. M. van Lerberghe, K. M. Motsegood, D. J. Beebe, *J. Microelectromech. Syst.* **2000**, *9*, 76.

[8] a) J. Cesarano III, P. D. Calvert, *US Patent 6 027 326*, **2000**. b) Q. Li, J. A. Lewis, *Adv. Mater.* **2003**, *15*, 1639. c) J. E. Smay, J. Cesarano III, J. A. Lewis, *Langmuir* **2002**, *18*, 5429. d) J. E. Smay, G. M. Gratson, R. F. Sheperd, J. Cesarano III, J. A. Lewis, *Adv. Mater.* **2002**, *14*, 1279.

[9] D. Therrriault, *Ph.D. Thesis*, University of Illinois at Urbana-Champaign **2003**.

Bioactive Hydrogels with an Ordered Cellular Structure Combine Interconnected Macroporosity and Robust Mechanical Properties**

By *Agnieszka N. Stachowiak*, *Anna Bershteyn*, *Elina Tzatzalos*, and *Darrell J. Irvine**

Bioactive hydrogels that consist of a cellular structure of interconnecting macropores combine tissue-like elasticity with enhanced pathways for mass transport and cell migration, making them attractive scaffolds for drug delivery and tissue engineering.[1–4] However, in order to obtain high degrees of pore interconnectivity using available stochastic porogen methods, void fractions exceeding 95 % must be introduced,[5–8] severely impacting mechanical properties such that a limited selection of stiff materials can be utilized.[3,9] Here we report a method to prepare soft hydrogels with interconnected porosity at moderate void fractions, thus maintaining a compressive stiffness that is comparable to native tissues. This was achieved by fabricating gels with ordered, interconnected macrovoids (20–60 μm diameter) via colloidal-crystal templating. The templated bioactive hydrogels supported cell attachment and migration through the interconnected structure. Two ubiquitous biomaterials, crosslinked poly(ethylene glycol) and gelatin, were templated; the generality of the approach should make it applicable to materials of interest for a broad range of bioengineering applications.

Colloidal-crystal templating has been extensively applied for the fabrication of photonic crystals, membranes, chromatography media, and solid-phase catalysis substrates.[10–13] The template is comprised of a crystalline arrangement of monodisperse microspheres (typically silica or polystyrene), which can

[*] Prof. D. J. Irvine, A. N. Stachowiak, A. Bershteyn
Department of Materials Science & Engineering
Massachusetts Institute of Technology
Cambridge, MA 02139 (USA)
E-mail: djirvine@mit.edu
Prof. D. J. Irvine
Biological Engineering Division
Massachusetts Institute of Technology
Cambridge, MA 02139 (USA)
E. Tzatzalos
Department of Chemical Engineering
Massachusetts Institute of Technology
MIT Room 8–425
77 Massachusetts Ave.
Cambridge, MA 02139 (USA)

[**] This work was supported by the Whitaker Foundation (grant number RG-02-0837). AS was supported by a National Defense Science and Engineering Graduate fellowship. We thank Lorna Gibson, Don Galler, Brendan Harley, and Nicki Watson (Keck Imaging Facility, Whitehead Institute) for helpful discussions. Supporting Information is available online from Wiley InterScience, or from the authors.

 DOI: 10.1002/adma.200400507